2862 *Chem. Mater.* **2009,** *21,* 2862–2867
DOI:10.1021/cm900565a

CHEMISTRY OF MATERIALS
Article

$WO_3-Fe_2O_3$ Photoanodes for Water Splitting: A Host Scaffold, Guest Absorber Approach

Kevin Sivula,* Florian Le Formal, and Michael Grätzel*

Institut des sciences et ingénierie chimiques, Ecole Polytechnique Fédérale de Lausanne, CH-1015 Lausanne, Switzerland

Received February 26, 2009. Revised Manuscript Received May 6, 2009

Solar hydrogen production via watersplitting with hematite (Fe_2O_3) has been limited by poor light absorption and a small hole diffusion length. These drawbacks can be overcome by using a high-surface-area host to support a thin layer of hematite—allowing photogenerated holes to be produced in high proximity to the semiconductor-liquid junction. Here we demonstrate the effectiveness of this concept using a nanostructured host scaffold (WO_3) prepared by atmospheric pressure CVD to support a thin layer of Fe_2O_3 nanoparticles deposited by a similar method. A 20% increase in the photocurrent was observed in host−guest electrodes as compared to control films with the same amount of hematite (equivalent to a 60 nm film) deposited without the host scaffold. The improvement is attributed to an increase in the absorbed photon conversion efficiency (APCE), especially for longer wavelengths where the photon penetration depth is large in hematite. For light with a wavelength of 565 nm, the APCE improves to 8.0%, as compared to 5.7% with the control films because of the host/guest architecture.

Introduction

The ultimate goal of the photoelectrochemist remains the efficient and sustainable splitting of water using solar illumination as the only energy input. Surmounting this challenge would not only represent significant achievement in the fields of materials science and electrochemistry but would also provide a means to convert energy from our most abundant renewable source, the sun, into dihydrogen, which would then be employed as an energy vector in a carbon-neutral market.[1] Indeed, interest in photoelectrochemical (PEC) water splitting into molecular hydrogen and oxygen intensified at the advent of the petroleum crisis in the 1970s, and was first demonstrated with a semiconductor−liquid junction (SCLJ) using TiO_2 as a photoanode in 1972.[2] Since this seminal demonstration, the search has continued for a PEC water splitting material combining efficient solar light harvesting, high quantum efficiency, practical durability, and low cost.[3] However, no single semiconducting material has yet been found to meet all of these requirements. Although systems delivering high efficiency have been demonstrated using III−V semiconductor materials with optimized band gaps and energy levels straddling the hydrogen and oxygen redox potentials, their cost and stability are a major disadvantage.[4] More stable oxide semiconductors like TiO_2 and WO_3 have been thoroughly investigated and optimized to deliver high single-wavelength quantum efficiencies.[5,6] Unfortunately, with their stability in aqueous environments also comes a large band gap that severely limits the fraction of solar illumination captured.

However, hematite (α-Fe_2O_3) remains a promising material. With a favorable band gap of 2.0−2.2 eV, chemical stability in aqueous environments, and matchless abundance, its use as a photocatalyst to produce dihydrogen at a scale corresponding to the world energy demand is realistic. Many research groups have examined this material as an oxygen-evolving photoanode for water-splitting in the past and have pointed out its limitations.[7−10] As a drawback, hematite possesses a conduction band edge at an energy level below the reversible hydrogen potential. Thus, any system implementing this material requires an external electrical bias to complete the water splitting reaction and bring about the desired hydrogen evolution at the cathode. However, by also using the solar photons with energy less than the band gap of hematite, unassisted solar hydrogen production can be achieved in a tandem cell configuration with, for example, a dye-sensitized solar cell (DSSC).[3]

*Corresponding author. E-mail: kevin.sivula@epfl.ch (K.S.); michael.graetzel@epfl.ch (M.G.).

(1) Turner, J. A. *Science* **2004**, *305*, 972.
(2) Fujishima, A.; Honda, K. *Nature* **1972**, *238*, 37.
(3) Gratzel, M. *Nature* **2001**, *414*, 338.
(4) Khaselev, O.; Turner, J. A. *Science* **1998**, *280*, 425.
(5) Ni, M.; Leung, M. K. H.; Leung, D. Y. C.; Sumathy, K. *Renewable Sustainable Energy Rev.* **2007**, *11*, 401.
(6) Santato, C.; Ulmann, M.; Augustynski, J. *J. Phys Chem. B* **2001**, *105*, 936.
(7) Dareedwards, M. P.; Goodenough, J. B.; Hamnett, A.; Trevellick, P. R. *J. Chem. Soc., Faraday Trans.* **1983**, *79*, 2027.
(8) Quinn, R. K.; Nasby, R. D.; Baughman, R. J. *Mater. Res. Bull.* **1976**, *11*, 1011.
(9) Sanchez, C.; Sieber, K. D.; Somorjai, G. A. *J. Electroanal. Chem.* **1988**, *252*, 269.
(10) Shinar, R.; Kennedy, J. H. *Sol. Energy Mater.* **1982**, *6*, 323.

Published on Web 06/08/2009

In addition, hematite has a very small hole diffusion length (2−4 nm)[11] as compared to the light penetration depth ($\alpha^{-1} = 118$ nm at $\lambda = 550$ nm).[12] This causes most photons to be absorbed in the bulk far from the SCLJ, creating photogenerated holes with low probability of participating in water oxidation. Recently, nanostructuring techniques have been proven useful in increasing the performance of hematite for water-splitting,[13] and several groups have reported various approaches.[14−16] Our group has reported benchmark performance with nanostructured and silicon-doped hematite thin films prepared by atmospheric pressure chemical vapor deposition (APCVD).[17] These state-of-the-art photoanodes possess a cauliflower-type morphology with feature sizes down to 5 nm and, when treated with a cobalt catalyst, exhibit a photocurrent of 2.3 mA cm^{-2} (1.8 mA cm^{-2} without cobalt) under simulated solar illumination (AM 1.5 G, 100 mW cm^{-2}) at an applied potential of 1.23 V vs the reversible hydrogen electrode (RHE), which corresponds to a solar-to-hydrogen conversion efficiency of more than 3% in a tandem configuration. However, this efficiency remains low compared to the theoretical value of 16.8% predicted for a material with this band-gap.[18] Even in this nanostructured system, the quantum conversion efficiencies are relatively low and are especially poor (<20%) in the region where hematite has an indirect band gap transition (λ = 610 − 450 nm). Importantly, there is more than 10 mA cm^{-2} of solar photocurrent available in this wavelength range. The poor performance here is largely due to the cauliflower-type morphology consisting of thick stems, which increase the number of photons absorbed far from the SCLJ. The present work aims to further develop this promising iron oxide system by overcoming this limitation.

An answer to the persisting problem of small hole diffusion length and large photon penetration depth proposed by Itoh and Bockris is to use ultrathin films in a stacked formation to increase the proximity of the photogenerated holes to the SCLJ.[19] While this solution could fundamentally resolve the issue, it is cumbersome and expensive to implement, and in practice the thin iron oxide films were found to have poor performance due to the increased recombination of the photogenerated holes.[20] An increased photoresponse should also be obtainable by coating these thin films conformally on a suitable nanostructured collector with a large specific surface area, in analogy to the DSSC.[21] In the case of the DSSC, the photoanode is constructed from a light-absorbing dye molecule anchored to a high-surface-area mesoporous TiO_2 scaffold, which transports and collects the photoexcited electrons. The DSSC's host-scaffold/guest-absorber approach effectively decouples light harvesting and charge transport while maximizing the incident photon-to-current efficiency (IPCE) by means of the thin (mono) layer of absorber on the high-surface-area, transparent collector. Given the success of this concept for photovoltaic energy conversion as well as the light-absorbing and carrier-transport limitations of α-Fe_2O_3, we sought to apply this powerful design to hematite photoanodes for PEC water splitting to improve on the silicon-doped photoanodes developed in our lab. Although reports of hematite-sensitized large-band gap oxides as photocatalysts have appeared,[22] no confirmation of the effectiveness of the host/guest concept for improving the quantum efficiency of hematite films for water-splitting has yet been demonstrated. Here we present affirmation that this approach can increase the photocurrent and absorbed photon conversion efficiency for thin-film hematite photoanodes using a nanostructured scaffold made from WO_3.

Experimental Section

To implement a host/guest architecture with hematite as the guest absorber, a scaffold host material must be chosen to fulfill a few essential requirements. First, the conduction band of the scaffold material must lie lower in energy than the conduction band of hematite to allow efficient electron transport across the host/guest interface and second, the scaffold material should have a larger band gap than hematite so as to not compete with the light absorption. Few oxide semiconductors meet both of these requirements. Both ZnO and SnO_2 have sufficiently large band-gaps (3.4 and 3.6 eV, respectively) and conduction bands close to that of hematite, but their investigations in composite architectures with hematite have not been effective, as the conduction band is too negative[23] for ZnO and recombination is increased at the SnO_2/hematite interface.[20,24,25] In addition, our unpublished investigations of other candidate materials (TiO_2, CoO, and Bi_2O_3) as scaffolds resulted in no photocurrent.

As previously mentioned, tungsten trioxide has been extensively investigated as a photoanode material. Although the experimental value of the conduction band of WO_3 varies slightly, it has been reported to be positioned 0.1−0.4 eV below that of hematite.[13,26] In addition, with a band gap of 2.7 eV, it satisfies the second criterion for a host material for λ > 460 nm. With this compliance, and the good electron conductivity shown by high photocurrents for WO_3,[6] we chose to investigate this material as a host scaffold.

(11) Kennedy, J. H.; Frese, K. W. *J. Electrochem. Soc.* **1978**, *125*, 709.
(12) Balberg, I.; Pinch, H. L. *J. Magn. Magn. Mater.* **1978**, *7*, 12.
(13) van de Krol, R.; Liang, Y. Q.; Schoonman, J. *J. Mater. Chem.* **2008**, *18*, 2311.
(14) Glasscock, J. A.; Barnes, P. R. F.; Plumb, I. C.; Savvides, N. *J. Phys. Chem. C* **2007**, *111*, 16477.
(15) Hu, Y. S.; Kleiman-Shwarsctein, A.; Forman, A. J.; Hazen, D.; Park, J. N.; McFarland, E. W. *Chem. Mater.* **2008**, *20*, 3803–3805.
(16) Liang, Y. Q.; Enache, C. S.; van de Krol, R. *Int. J. Photoenergy* **2008**, 739864.
(17) Kay, A.; Cesar, I.; Gratzel, M. *J. Am. Chem. Soc.* **2006**, *128*, 15714.
(18) Murphy, A. B.; Barnes, P. R. F.; Randeniya, L. K.; Plumb, I. C.; Grey, I. E.; Horne, M. D.; Glasscock, J. A. *Int. J. Hydrogen Energy* **2006**, *31*, 1999.
(19) Itoh, K.; Bockris, J. O. *J. Electrochem. Soc.* **1984**, *131*, 1266.
(20) Itoh, K.; Bockris, J. O. *J. Appl. Phys.* **1984**, *56*, 874.
(21) Gratzel, M. *Chem. Lett.* **2005**, *34*, 8.
(22) Liu, H. Y.; Gao, L. *J. Am. Ceram. Soc.* **2006**, *89*, 370.
(23) Glasscock, J. A.; Barnes, P. R. F.; Plumb, I. C.; Bendavid, A.; Martin, P. J. *SPIE Conf. Proc.* **2006**, *63400N*, 12.
(24) Cesar, I. Solar Photoelectrolysis of Water with Translucent Nanostructured Hematite Photoanodes; EPFL: Lausanne, Switzerland, 2007.
(25) Cesar, I.; Sivula, K.; Kay, A.; Zboril, R.; Gratzel, M. *J. Phys. Chem. C* **2009**, *113*, 772.
(26) Xu, Y.; Schoonen, M. A. A. *Am. Mineral.* **2000**, *85*, 543.

WO_3 Film Preparation. Given our experience with the APCVD of Fe_2O_3 from iron pentacarbonyl,[17] we chose a similar method to deposit thin films of WO_3 with high roughness to serve as the scaffold.[27] Thin films of WO_3 with high roughness were prepared on transparent conductive substrates ($F:SnO_2$, TEC15, 15 $\Omega\,\square^{-1}$, 60 mm × 60 mm × 2.3 mm) by the atmospheric pressure chemical vapor deposition of tungsten hexacarbonyl (99%, Acros) using the following procedure. The substrate was placed on a 3 mm thick slab of ceramic glass covering the surface of a PID-controlled high temperature hot plate (Harry Gestigkeit GMBH). The hot plate was heated to 400 °C, and a center strip of the conducting glass substrate (60 mm × 12 mm) was masked with an additional piece of glass for later electrical contact. The solid tungsten hexacarbonyl (500 mg) was spread evenly on a standard glass frit (40 mm dia.) of a vacuum filtration funnel assembly (70 mm funnel dia.). The inverted vacuum filtration funnel assembly with the $W(CO)_6$ was placed over the substrate so the top of the funnel was 50 mm from the substrate. A 7.1 L min^{-1} flow of dry air that had been heated to 120 °C by PID-controlled thermal resistant heaters was directed into the stem of the funnel assembly, over the $W(CO)_6$, through the glass frit, and onto the hot substrate, where the pyrolytic decomposition of the tungsten hexacarbonyl vapor occurred. The entire amount of $W(CO)_6$ was allowed to sublime (about 15 min) and the substrate was subsequently annealed for 45 min more at the same temperature and flow of heated air. The substrate was cooled and diced into 30 mm × 12 mm pieces for the iron oxide deposition. The films were uniform, slightly yellow with increased haze as compared to the TEC15 substrate.

APCVD of $Si:Fe_2O_3$. These films were then subjected to the APCVD of silicon-doped Fe_2O_3 from iron pentacarbonyl and tetraethyl orthosilicate (TEOS) in a cold wall APCVD chamber. For this work we constructed a new deposition system, based on our previous work,[17] which offered increased parameter control plus improved stability and reproducibility over the former system. Further details and are included in the Supporting Information. The deposition of α-Fe_2O_3 at approximately 100 nm min^{-1} (after a latency time)[25] at a substrate temperature of 420 °C resulted in a red-orange spot approximately 1 cm in diameter on the substrate. Depositions were performed for 1 or 4 min on both the WO_3 films and, as a control, on the bare $F:SnO_2$ substrates without any surface treatment.

Photocurrent Measurements. Photocurrent measurements were performed to determine the solar to hydrogen energy conversion efficiency in a three-electrode configuration with 1 M NaOH (pH 13.6)[11] as electrolyte using Ag/AgCl in saturated KCl as a reference electrode. The hematite electrode was scanned at 50 mV sec^{-1} between −300 and 800 mV vs Ag/AgCl. The potential is reported relative to the reversible hydrogen electrode potential (RHE).[17] The samples were illuminated with simulated sunlight from a 450 W xenon lamp (Osram, ozone free) using a KG3 filter (3 mm, Schott). Spectral mismatch factors to estimate the difference of the electrode photoresponse obtained from simulated sun light and real sun light at AM 1.5 G were calculated according to the method described by Seaman et al.[28] Photocurrent action spectra and the UV−vis transmittance were measured to determine the absorbed photon to current conversion efficiency (APCE). Photocurrent action spectra were obtained under light from a 300 W Xe-lamp with integrated parabolic reflector (Cermax PE 300 BUV) passing through a monochromator (Bausch & Lomb, bandwidth 10 nm fwhm). The photoanode transmittance was measured on a Hewlett-Packard 8452A diode array spectrophotometer. A detailed description of the setup and determination of the APCE is found elsewhere.[25] All samples were measured by illuminating the photoanode from the hematite/electrolyte interface.

Results and Discussion

Scanning electron micrographs (Figure 1) of the WO_3 and the WO_3/Fe_2O_3 films give insight to the nanostructured morphology obtained by our deposition techniques. Figure 1a shows the surface morphology of the WO_3 film before the iron oxide deposition. The film consisted of faceted grains of WO_3 in the size range of 20−200 nm grown from the surface $F:SnO_2$ substrate creating a porous structure with increased roughness over the underlying substrate (see Figure S1 in the Supporting Information). Upon the deposition of the iron oxide for 1 min, the WO_3 scaffold was completely covered with ca. 10 nm particles of silicon-doped iron oxide (Figure 1c); however, some of the original porosity can be distinguished, suggesting the iron oxide deposits conformally on the WO_3. This is remarkable given the homogeneous-nucleation-and-attachment growth mechanism supposed for this deposition[25] and is further indicated by observing a position on the film near the edge of the iron oxide deposition spot (Figure 1b). Here we note the rounded iron oxide nanoparticles beginning to attach to all sides of the WO_3 surface and can subsequently suggest that surface nucleation may be critical to the nanostructure obtained from the APCVD of Fe_2O_3 from carbonyl. Finally, a cross-sectional micrograph (Figure 1d) reveals the rounded iron oxide nanoparticles covering the faceted WO_3 nearly down to the $F:SnO_2$ substrate. The observed film thickness of ca. 300 nm is consistent with a 200 nm WO_3 film accounting for the additional height of the Fe_2O_3.

To quantify the effectiveness of the WO_3/Fe_2O_3 host/guest approach for water splitting the photoanodes were analyzed independently from a tandem system as the working electrode in a potentiostatic cell with 1 M NaOH (pH 13.6)[29] as the electrolyte, a Pt counter electrode, and an Ag/AgCl reference electrode. The current density, corresponding to oxygen evolution at the photoanode SCLJ, as a function of potential with respect to RHE of the 1 and 4 min iron oxide depositions are shown in Figure 2 in the dark and in simulated sunlight (AM 1.5G, 100 mW cm^{-2}). In general, when scanned in the anodic direction, the electrode's dark current remains small until the onset of water electrolysis around 1.6 V_{RHE}. Under illumination, the photo current increases sharply around 1.0 V_{RHE} and reaches a plateau before the onset of the dark current. For electrodes prepared with a 1 min iron oxide deposition (Figure 2a), we see a significant increase in the photocurrent plateau in the WO_3/Fe_2O_3

(27) Tanner, R. E.; Szekeres, A.; Gogova, D.; Gesheva, K. *Appl. Surf. Sci.* **2003**, *218*, 162.
(28) Seaman, C. H. *Sol. Energy* **1982**, *29*, 291.
(29) Kennedy, J. H.; Frese, K. W. *J. Electrochem. Soc.* **1978**, *125*, 723.

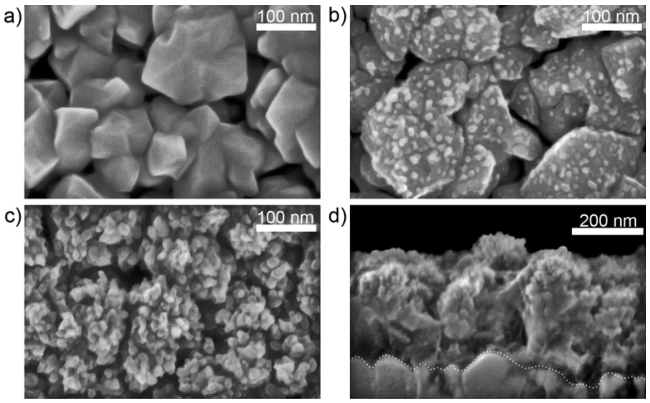

Figure 1. Scanning electron micrographs of the WO_3/Fe_2O_3 host/guest system in a (a–c) top-down and (d) cross-sectional perspective. (a) Morphology of the WO_3 host scaffold before iron oxide deposition. (c) After 1 min of Fe_2O_3 deposition at the standard deposition rate ($\sim$100 nm min^{-1}), the WO_3 film is covered in iron oxide nanoparticles, whereas (b) at a lower deposition rate ($\sim$10 nm min^{-1}, edge of growth spot), the iron oxide nanoparticles are seen just starting to cover the WO_3 scaffold. (d) The cross-section of the WO_3/Fe_2O_3 film, corresponding to c. The broken white line indicates the $F:SnO_2/WO_3$ interface.

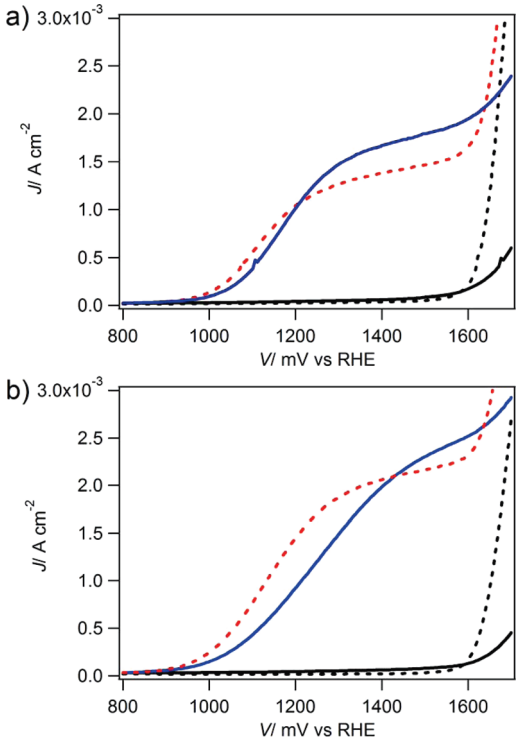

Figure 2. Current densities, J, of the prepared photoanodes in the dark (black curves) and under simulated solar illumination (colored curves) are shown as a function of the applied potential, V, with respect to the reversible hydrogen electrode (RHE). Electrode performance with a Fe_2O_3 deposition time of (a) 1 and (b) 4 min. The host/guest ($F:SnO_2/WO_3/Fe_2O_3$) and the control ($F:SnO_2/Fe_2O_3$) electrode current densities are indicated by solid (blue) and broken (red) lines, respectively.

photoanode over the control electrode prepared without the WO_3 scaffold (1.71 and 1.41 mA cm^{-2}, respectively, at 1.43 V_{RHE} corresponding to a 21% increase). This effect is reduced upon longer deposition times (4 min, Figure 2b) because of the increased thickness of the iron oxide guest layer. However, increased photocurrent was still observed after this longer deposition time at voltages approaching the dark current onset. The observed photocurrent increase using the host/guest electrodes in Figure 2 was reproducible on several repeat samples and was stable for multiple scans of each photoanode despite tungsten trioxide's solubility in aggressively basic solutions. Although extensive stability testing was not performed, this result suggests the iron oxide could effectively protect the WO_3 from contact with the electrolyte.

In addition to quantifying the performance with the photocurrent plateau value, the photocurrent onset behavior can give indication of the differences in photoanode operation. In both the 1 and 4 min iron oxide depositions, we observe a minimal shift in the photocurrent onset potentials (1.00 V_{RHE} for the control vs 1.03 V_{RHE} for the host/guest for both deposition times), a slight change that may be due to small barrier for electron transport over the Fe_2O_3/WO_3 interface. Moreover, the difference between the rise of the photocurrent (as characterized by the Tafel slope, see the Supporting Information) is indistinguishable for both electrodes after 1 min of iron oxide deposition, indicating matching water oxidation kinetics. However, the Tafel slope increases dramatically from 174 (control) to 209 mV $decade^{-1}$ for the host/guest electrode after 4 min of deposition, which indicates increased nonideality in the photocurrent onset.[30] This result could be due to the rough scaffold's influence on fully developing the cauliflower-type morphology and the previously observed crystalline alignment[17] associated with these iron oxide films after 4 min of deposition and is consistent with our observations depositing on $F:SnO_2$ with increasing roughness. Finally, we note the change in the dark current onset, which in the control case occurs at 1.6 V_{RHE} as previously reported. With the host/guest photoanodes the dark current becomes significant at the same potential, but has more gradual onset due to the WO_3 scaffold, demonstrating a strong effect of the scaffold on the dark current.

An increased photocurrent is expected using the host/guest approach for hematite over our previous cauliflower-type nanostructure because more of the iron oxide is closer to the hematite/electrolyte interface, allowing a greater fraction of the photoproduced holes to transfer to the SCJL and participate in water oxidation. The beneficial effects of the host/guest morphology should be diminished if the thickness of the guest layer far exceeds the photoexcited carrier transport length. Our observed photocurrent results with 1 and 4 min iron oxide depositions are consistent with this hypothesis. However, it is possible that the increase in photocurrent for the 1 min deposition is wholly a result of the presence of more iron oxide due to the greater surface area of the scaffold material. In addition, because the goal of the host/guest approach is to increase the internal quantum efficiency of the guest material, especially in the wavelength region near the absorption band edge, proper confirmation of the effectiveness of the WO_3/Fe_2O_3 host guest approach should come from examining the quantum efficiency of

(30) Wang, H. L.; Lindgren, T.; He, J. J.; Hagfeldt, A.; Lindquist, S. E. *J. Phys. Chem. B* **2000**, *104*, 5686.

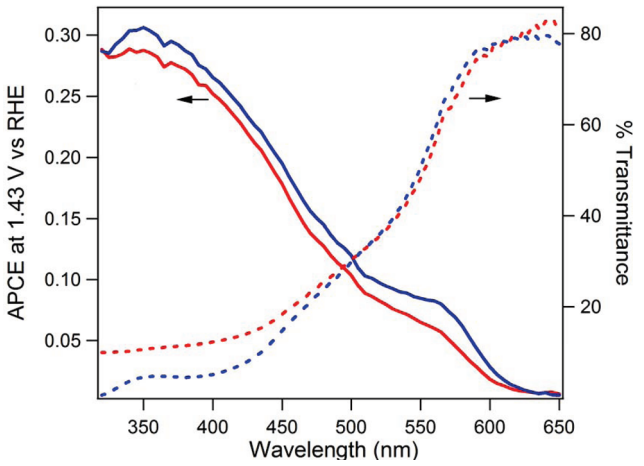

Figure 3. Absorbed photon to current efficiency, APCE, (solid lines) at 1.43 V_{RHE} and the percent transmittance, *T*, (broken lines) of photoanodes prepared with a 1 min Fe_2O_3 deposition time plotted against the incident light wavelength, λ. The host/guest ($F:SnO_2/WO_3/Fe_2O_3$) and the control ($F:SnO_2/Fe_2O_3$) electrode responses are indicated by blue and red lines, respectively.

these electrodes. To this end, we acquired photoaction and UV−vis transmittance spectra of the host/guest and control electrodes from the 1 min iron oxide deposition. The internal quantum efficiency of the electrodes was then estimated by calculating the absorbed photon to current efficiency (APCE) as previously described.[25] The results for the electrode transmittance and APCE acquired at a potential on the photocurrent plateau (1.43 V_{RHE}) as a function of the illumination wavelength for the 1 min films are shown in Figure 3.

The transmission spectra of the host/guest and control electrodes show a practically identical light absorption by the two films in the region where only iron oxide is absorbing (500−600 nm). This indicates that there is the same amount of iron oxide in both of the 1 min films, and interestingly, suggests that the deposition rate of iron oxide does not depend on the roughness of the substrate during the first minute. In the wavelength band from 350 to 500 nm, the transmittance of the host/guest electrode is found to decrease more compared to the control electrode due to the increased absorbance of the WO_3 scaffold. Because the penetration depth of photons in iron oxide increases beyond 100 nm near the band edge, these photons are generally absorbed deep within the iron oxide film, but because of the host/guest architecture, more of the iron oxide should be closer to the SCLJ and the quantum efficiency of the longer wavelengths should be increased over that of a cauliflower-type structure. Indeed, comparing the APCE of the host/guest electrode to the control confirms this and the effectiveness of the host/guest approach. An increased APCE is observed over all photon energies, which could be explained by better electron transport through the host/guest architecture. However, near the band edge from 2.1 to 2.5 eV (600−500 nm) the improvement of the APCE increases significantly more, reaching a maximum of 40% (8.0 and 5.7%, respectively, for the host/guest and control, respectively) at 565 nm. Because this extra improvement is observed only for wavelengths near the band edge, we can presume it is due to the facilitation of photogenerated holes to the SCLJ. In addition, there is no disproportionate increase in the APCE of the host/guest photoanode around 460 nm (2.7 eV), eliminating the possibility that the increased photocurrent observed is due to light absorption by WO_3 followed by hole transfer to the Fe_2O_3. Another possible explanation for the increased performance of the iron oxide is the incorporation of some of the tungsten from the scaffold. It is true that hematite photoanodes are very sensitive to small levels of impurities. However, it is unlikely in this case because of the relatively low synthesis temperatures and preferential increase in the quantum efficiency at the longer wavelengths. We would expect an equal increase of the performance for all wavelengths if a tungsten dopant was playing an important role. Still, an interesting feature of the APCE trace is observed in this and previous work as an abrupt change in slope at 500 nm (2.5 eV) for both cases. In our improved host/guest electrode, the APCE enhancement seems to be greatest for photon energies lower than this value. Hematite is reported to have direct electronic transition at $\lambda < 400$ nm (O^{2-} $2p^6 \rightarrow Fe^{3+}$ 3d) and an indirect transition between 400 and 620 nm (Fe^{3+} 3d → 3d).[7] However, we are not able to explain this transition at 500 nm, but as it is clearly an important feature of APCE results for the host/guest approach, we are actively working to understand this attribute.

The increased photocurrent and APCE data presented here represent the initial demonstration of the host/guest approach to enhance photon harvesting in hematite for photoelectrochemical water-splitting. Although the improvement observed is modest, it represents an important first step in the complex nanostructuring that will be necessary to fully realize the potential of hematite. Further improving the quantum efficiency of hematite using the host/guest approach will be accomplished by using an even thinner layer of iron oxide. This, coupled with an increased roughness and porosity of the scaffold layer, should allow the increase in the photocurrent above the state-of-the-art reported for hematite. However, the depositions methods that have been shown to be most effective for this material exhibit a photoinactive "dead" layer near the interface with the substrate.[25] This manifests as a negligible photocurrent for the thinnest films. Although our results for the 1 min films suggest some improvement of this dead layer, our efforts to deposit even thinner layers of hematite on the WO_3 scaffold with the APCVD method gave results consistent with interfacial limitations; this issue needs to be addressed by either interfacial engineering or identifying a suitable deposition method that allows even thinner films of hematite to be photocatalytically active toward water splitting. Our current efforts concern these goals.

Conclusion

We have shown that host/guest approach, already successfully employed for other electrochemical systems

like the DSSC, can be applied to hematite for photoelectrochemical water splitting. A ca. 20% increase in photocurrent was observed when using WO_3/Fe_2O_3 host/guest photoanodes as compared to control devices. Accordingly, increased quantum efficiency, especially from wavelengths near the hematite absorption edge where photons have long penetration depths, was also observed, as a greater fraction of photons could be absorbed closer the hematite/electrolyte interface. Continued perfection of the nanostructure while also addressing the limiting interfacial issues will no doubt allow the host/guest approach to reveal the full potential of hematite for solar hydrogen production in a tandem cell system.

Acknowledgment. We thank the Swiss Federal Office of Energy (Project number 102326, PECHouse) and the Marie Curie Research Training Networks (Contract number MRTN-CT-2006-032474) for financial support. We also acknowledge P. Chen and the Centre Interdisciplinaire de Microscopie Electronique at the EPFL and for assistance in SEM imaging and R. Robert and A. Weidenkaff at EMPA for thin film XRD characterization.

Supporting Information Available: The complete experimental procedure for the APCVD of Fe_2O_3, addition characterization of the WO_3 scaffold by SEM and XRD, and electrode Tafel behavior (PDF). This material is available free of charge via the Internet at http://pubs.acs.org.